Magnetoelectric Versus Inductive Power Delivery for Sub-mm Receivers

Adam Khalifa[1], Mehdi Nasrollahpour[2], Neville Sun[2], Mohsen Zaeimbashi[2], Huaihao Chen[2], Xianfeng Liang[2]
Milad Alemohammad[3], Ralph Etienne-Cummings[3], Nian X. Sun[2], Sydney Cash[1]
[1]Department of Neurology, Massachusetts General Hospital, Harvard Medical School, USA.
[2]Department of Electrical and Computer Engineering, Northeastern University, USA.
[3]Department of Electrical and Computer Engineering, Johns Hopkins University, USA.
Email: {akhalifa1@mgh.harvard.edu}

2021 IEEE Wireless Power Transfer Conference (WPTC) | 978-1-7281-9633-6/20/$31.00 ©2021 IEEE | DOI: 10.1109/WPTC51349.2021.9458201

***Abstract*—Most of the next-generation implantable medical devices that are targeting sub-mm scale form factors are entirely powered wirelessly. The most commonly used form of wireless power transfer for ultra-small receivers is inductive coupling and has been so for many decades. This might change with the advent of novel microfabricated magnetoelectric (ME) antennas which are showing great potential as high-frequency wireless powered receivers. In this paper, we compare these two wireless power delivery methods using receivers that operate at 2.52 GHz with a surface area of 0.043 mm^2. Measurement results show that the maximum achievable power transfer of a ME antenna outperforms that of an on-silicon coil by approximately 7 times for a Tx-Rx distance of 2.16 and 3.3 times for a Tx-Rx distance of 0.76 cm.**

***Index Terms*—Power transfer efficiency, RF, magnetoelectric, on-chip coil, miniaturization, biomedical.**

I. Introduction

Sub-mm wirelessly-powered devices play a major role in emerging applications such as: *i)* Implantable medical devices (IMDs) used for neural monitoring [1], neural stimulation [2], [3], cell tracking [4], intraocular pressure [5] and glucose monitoring [6]; and *ii)* RFID tags placed on electronic devices to eliminate counterfeit ICs from the supply chain [7], [8]. Aggressive miniaturization of these devices opens up new possibilities and offers multiple advantages with respect to safety, longevity, spatial resolution, and security.

Multiple wireless powering modalities exist in the sub-mm scale, with near/mid-field and ultrasonic being the main ones. Although each method offers trade-offs (Fig. 1), inductive coupling has the important advantage of using coils that can be microfabricated on-silicon chips leading to highly miniaturized receivers (Rx) [2], [9]–[11].

Recently, sub-mm scale magnetoelectric (ME) antennas have been shown to allow one of the highest power transfer efficiencies (PTE) reported to date [12], [13]. Acoustically actuated ME antennas seem to provide a good balance between miniaturization capability (the microfabrication extent to which it can be made very small) and power transfer efficiency (Fig. 1). In addition, they offer the advantage of being less sensitive to Tx-Rx misalignment and can potentially eliminate the need for matching networks [12], [14]. The ME antennas incorporate a magnetic and piezoelectric heterostructure where the magnetic film senses H-components of EM waves. The magnetic layer then induces an oscillating strain, which generates a piezoelectric voltage output at the electromechanical resonance frequency. By exploiting this transduction mechanism, ME antennas do not suffer from the same miniaturization constraints as coils or piezo transformers, and weak magnetic fields can drive them.

Unfortunately, previous publications on sub-mm sized ME antennas do not directly compare efficiency between ME and inductive coupling. This is because the *i)* testbench setups were different between the coil and ME antenna; *ii)* efficiency measurements often included that of matching networks and harvesting circuits; and *iii)* comparisons were based on simulations results.

For the first time, we compare inductive to magnetoelectric power delivery for sub-mm receiving devices using the same testbench setup, operating frequency, and receiver size. This makes the comparison of the two systems equitable. In our calculations, we ignore the load, as the optimum load can always be realized using matching networks with only a few percent penalties in efficiency.

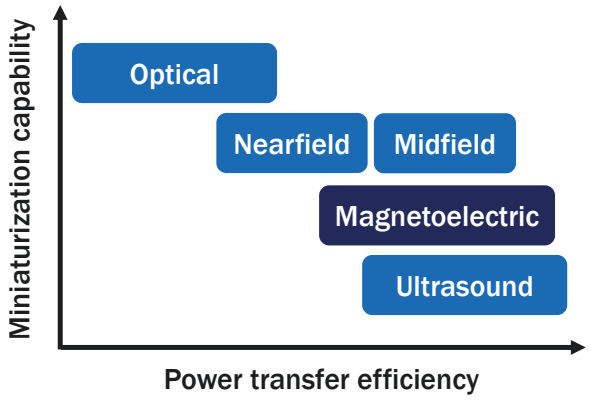

Figure 1. Qualitative comparison between different wireless powering methodologies for sub-mm implantable receivers.

II. Transmitter and Receiver Design

A. Transmitter Coil

The Tx coil is designed based on an optimized design flow described in [2]. Details of its geometry and parameters are

shown in Table II. The Tx coil was built on an FR4 substrate and is connected to an L-match capacitor network. The Tx coil diameter is chosen to maximize powering for receivers placed approximately 1 cm away.

B. Receiver Coil

The Rx coil is designed based on an optimized design flow described in [2]. The major goal was to maximize the quality factor (Q) as much as possible at the operating frequency of 2.52 GHz. The on-chip coil was fabricated in 65nm TSMC CMOS process and measures 216 µm × 200 µm, giving it a surface area of 0.0432 mm^2. Details of its geometry and parameters are shown in Table II.

An integrated circuit (IC) pad frame often includes a compulsory seal ring which contains all the metal layers available in the fabrication process with uninterrupted continuous contacts and vias. It has been shown that the grounded seal ring significantly diminishes the gain of an on-chip coil as any metal loop can create a magnetic field that counters that of the source [15]. In order to eliminate the impact of the seal ring on the PTE, the received die from the foundry is further diced in such a way as to leave only the on-chip coil and the pads needed for its interface, as shown in Fig. 2.

A variable on-chip capacitor to enable resonance was not added to the chip, as it would have increased the interfacing complexity which would have increased the electromagnetic interference (EMI). The impact of EMI on the PTE is further discussed in the following sections. Furthermore, a resonating coil would not have made a difference since we are only measuring the maximum achievable PTE in this paper.

C. Receiver Magnetoelectric Antenna

The ME antenna is designed based on an optimized design flow described in [12]. It measures 250 µm × 174 µm, giving it a surface area of 0.0435 mm^2. The resonant frequency was set to 2.52 GHz by adjusting the thickness of the multiferroic antenna.

Because the ME antenna is composed of a thin-film bulk acoustic wave resonator (FBAR) that is released to prevent damping of the acoustic vibration, dicing around a single ME antenna using a dicing saw is not possible as the vibration and water jet will damage the antenna. Therefore, we manually diced the substrate using a diamond scriber to reduce its size down to 700 µm × 560 µm, which significantly reduces any EMI captured by the neighboring antennas on the silicon chip.

III. Wireless Link Characterization

A. Measurement Method

One possible test-bench setup would have been to wirebond the receivers to a PCB. In conventional inductive links with cm-sized Rx coils, the measured PTE are reasonably accurate, because the effect of the SMA connector, interconnects, and wirebonds are quite negligible. However, a major inconvenience when characterizing sub-mm sized receivers and transmitting power at a very short distance from the test board is the unwanted EMI in the PCB traces and wire bonds and the magnetic field disturbance caused by the relatively large conductive body of the SMA connector. We have attempted to characterize their effect in past work [15], but fully understanding their link on the measured efficiency is challenging. Therefore, to minimize the distortion caused by electromagnetic interference on the efficiency, the receivers were directly interfaced using a probe station (Fig. 3).

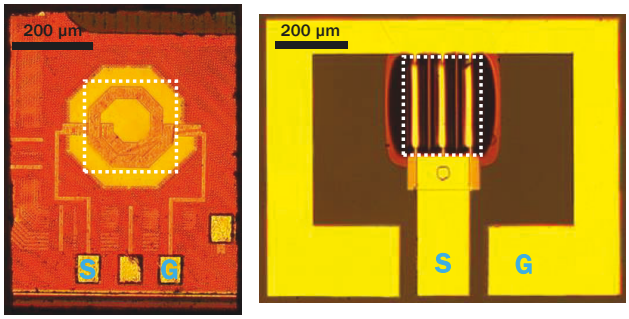

Figure 2. Micrograph image of the on-chip coil (left) and ME antenna (right) after dicing. The white rectangular doted line encircles the coil and the antenna, everything outside the rectangle represents interconnects and pads needed for probing.

The Tx coil is held using a 3D printed plastic manipulator in order to eliminate its effect on the wireless link. The platform that supports the substrates is also 3D printed. The only metallic objects surrounding the antenna/coil are the GS probe and the station. The Tx coil and the probe are both connected to a VNA to measure the S-parameters, as shown in Fig. 3(a) The Tx-Rx distance is precisely controlled with 2.16 cm as the upper limit. Large Tx-Rx distances are not investigated in this work as we are only interested in the reactive near field region. As shown in Fig. 3(b), 3D printed photopolymer pillars were used in order to improve the angular alignment of the Tx coil and to guarantee a certain distance between the Tx coil and Rx coil/antenna. For accurate measurements, the parasitic effect caused by the coaxial cable and the GS probe were removed during the de-embedding calibration procedure. De-embedding was also done for the Tx coil. Table I shows that the setup used for measuring the wireless link is almost identical between inductive and magnetoelectric systems. We made this a priority in this work in order to enable a fair and equitable performance comparison between the two dissimilar technologies.

The full system efficiency (η_{link}) is defined as the ratio of power delivered to the resistive load (P_L) to the transmitted source power set by the power generator (P_S). Therefore, the overall efficiency includes several loss factors, which are the power loss: *i)* in the Tx coil (η_{TxCoil}), which includes that of the power amplifier (PA) and coaxial cable, *ii)* between the Tx and Rx coil (PTE_{max}), and *iii*) in the Rx coil (η_{RxCoil}), which includes power reflected due to impedance mismatch. The product of all efficiencies is given by:

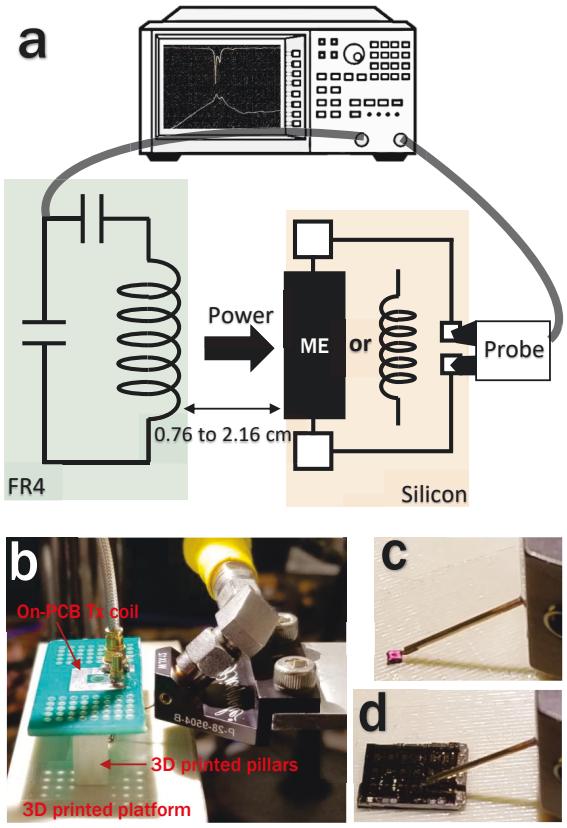

Figure 3. (a) Block diagram, and (b) picture of the PTE measurement setup. Close-up view of the silicon substrate containing the (c) coil, and (d) ME antenna.

$$\eta_{link} = \frac{P_L}{P_S} = \eta_{TxCoil} * PTE_{max} * \eta_{RxCoil}$$

The maximum achievable efficiency (PTE_{max}) is outlined in detail in [16] and is given by:

$$PTE_{max} = \frac{\chi}{(1+\sqrt{1+\chi})^2}$$

$$\chi = \frac{|Z_{12}|^2}{Re(Z_{11})Re(Z_{22}) - Re(Z_{12})^2}$$

Z represents the two-port impedance parameter matrix from the input of the Tx coil to the output of the Rx coil/antenna.

The most important step toward maximizing the wireless link (η_{link}) is maximizing the maximum achievable efficiency (PTE_{max}) since the impedance mismatch can almost be eliminated by using a tunable matching network. In this work, we are solely interested in the ability of the ME antenna and on-chip coil to receive power, and not its ability to transfer the captured power to a particular load. Therefore, in order to effectively compare both receivers, only PTE_{max} is calculated and plotted.

Table I
SETUP COMPARISON BETWEEN RX COIL AND ME ANTENNA.

Parameter	Similarities
Rx Area	similar
Frequency	same
Tx Coil used	same
Tx-Rx distance	same
Parasitics	similar
Probes	same

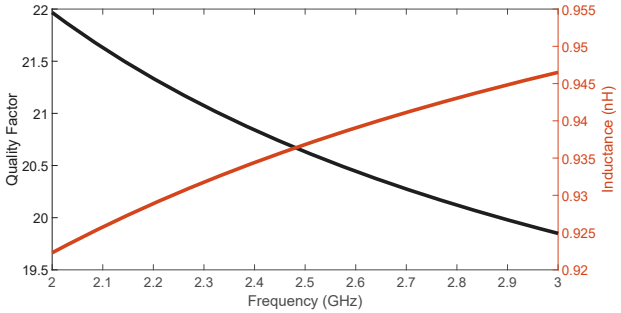

Figure 4. Measured quality factor and effective inductance of the 200 µm on-silicon coil.

Table II
CHARACTERIZATION OF THE TX COIL, RX COIL AND RX ME ANTENNA

Parameter	Tx Coil	On-chip Coil	ME Antenna
Dimensions (mm^2)	10×10	0.216×0.2	0.25×0.174
Material	*Cu*	*Al*	*FeGAB/AlN*
Trace width (mm)	3	28e-3	*N/A*
Trace thickness (µm)	35.6	3.4e-3	*N/A*
Space between turns (mm)	*N/A*	2.4e-3	*N/A*
Number of turns	1	1.5	*N/A*
f_{res} (GHz)	2.52	2.52	2.52
Q at f_{res} in air	155	20.65	104.2
L at f_{res} in air (nH)	10	0.94	*N/A*
SRF (GHz)	4.1	30	*N/A*

B. Measurement Results

As shown in Fig. 4, the measured quality factor of the Rx coil is 20.65 at 2.52 GHz which is considered to be very high for a 200 µm coil microfabricated on-silicon [17]. Therefore, it is important to note that the ME antenna is compared to a highly optimized on-chip coil.

Fig. 5 shows the PTE_{max} as a function of frequency for different distances. The maximum achievable power transfer efficiency of the ME antenna outperforms that of an on-silicon coil by approximately 7 times for a Tx-Rx distance of 2.16 cm and 3.3 times for a Tx-Rx distance of 0.76 cm.

The effects of angular misalignment were also explored by tilting the Rx by 90°. Fig. 6 shows that an out of plane rotation along the width direction of the ME antenna

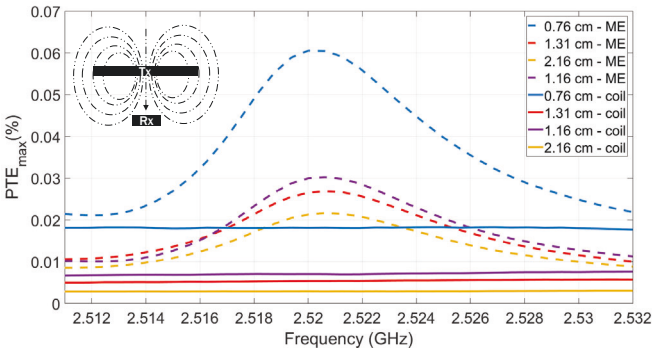

Figure 5. Measured maximum achievable PTE as a function of frequency for different Tx-Rx values. Doted lines represent the ME antenna whereas solid lines represent the on-chip coil.

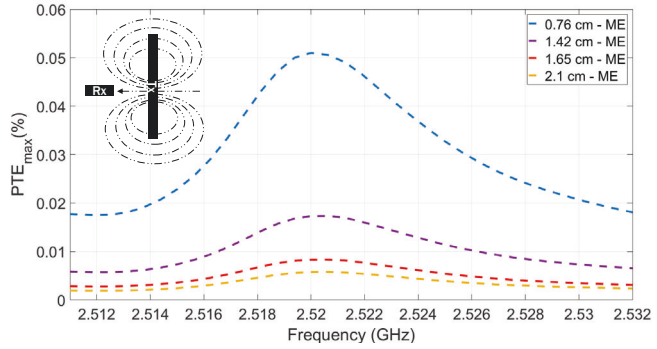

Figure 6. Measured maximum achievable PTE as a function of frequency for different Tx-Rx values when the Tx coil and ME anntena are rotationally mislaigned by 90˚.

does not significantly decrease the PTE_{max}. This has been demonstrated to some degree in our past work [18] for the far field configuration. On the other hand, when the angle between the Tx coil and the Rx coil is exactly 90˚, none of the magnetic flux passes through the Rx coil and the two coils are completely decoupled. As a result, the negligible harvested energy is below the noise floor of the VNA and is thus not included in the plot.

IV. Conclusion

We compare the maximum achievable efficiency (the efficiency calculated under the condition of maximum power transfer to the load) between a 0.0435 mm^2 ME antenna to a 0.0432 mm^2 on-silion coil. The results show that the magneto-electric power delivery outperforms the inductive one, making the ME antenna very attractive for miniaturized wirelessly powered microdevices, particularly for miniature IMDs for which the major challenge is transferring energy wirelessly over several centimeters. It is important to note that the fabricated ME antenna and on-chip coil followed a certain optimized design flow and if design methods were to change then the difference in PTE between both systems will most likely change too.

References

[1] S. Lee, A. J. Cortese, A. Mok, C. Wu, T. Wang, J. U. Park, C. Smart, S. Ghajari, D. Khilwani, S. Sadeghi *et al.*, "Fabrication of injectable micro-scale opto-electronically transduced electrodes (motes) for physiological monitoring," *Journal of Microelectromechanical Systems*, vol. 29, no. 5, pp. 720–726, 2020.

[2] A. Khalifa, Y. Liu, Y. Karimi, Q. Wang, A. Eisape, M. Stanaćević, N. Thakor, Z. Bao, and R. Etienne-Cummings, "The microbead: A 0.009 mm3 implantable wireless neural stimulator," *IEEE Transactions on Biomedical Circuits and Systems*, vol. 13, no. 5, pp. 971–985, 2019.

[3] D. K. Freeman, J. M. O'Brien, P. Kumar, B. Daniels, R. A. Irion, L. Shraytah, B. K. Ingersoll, A. P. Magyar, A. Czarnecki, and J. Wheeler, "A sub-millimeter, inductively powered neural stimulator," *Frontiers in neuroscience*, vol. 11, p. 659, 2017.

[4] X. Hu, K. Aggarwal, M. X. Yang, K. B. Parizi, X. Xu, D. Akin, A. S. Poon, and H.-S. P. Wong, "Micrometer-scale magnetic-resonance-coupled radio-frequency identification and transceivers for wireless sensors in cells," *Physical Review Applied*, vol. 8, no. 1, p. 014031, 2017.

[5] M. H. Ouda, M. Arsalan, L. Marnat, A. Shamim, and K. N. Salama, "5.2-ghz rf power harvester in 0.18μm cmos for implantable intraocular pressure monitoring," *IEEE Transactions on Microwave Theory and Techniques*, vol. 61, no. 5, pp. 2177–2184, 2013.

[6] M. H. Nazari, M. Mujeeb-U-Rahman, and A. Scherer, "An implantable continuous glucose monitoring microsystem in 0.18 μm cmos," in *VLSI Circuits Digest of Technical Papers, 2014 Symposium on*. IEEE, 2014, pp. 1–2.

[7] N.-C. Kuo, B. Zhao, and A. M. Niknejad, "Equation-based optimization for inductive power transfer to a miniature cmos rectenna," *IEEE Transactions on Microwave Theory and Techniques*, vol. 66, no. 5, pp. 2393–2408, 2018.

[8] L. Greenemeier, "The pentagon's seek-and-destroy mission for counterfeit electronics," *Scientific American*, vol. 28, 2017.

[9] N.-C. Kuo, B. Zhao, and A. M. Niknejad, "Equation-based optimization for inductive power transfer to a miniature cmos rectenna," *IEEE Transactions on Microwave Theory and Techniques*, vol. 66, no. 5, pp. 2393–2408, 2018.

[10] V. W. Leung, J. Lee, S. Li, S. Yu, C. Kilfovle, L. Larson, A. Nurmikko, and F. Laiwalla, "A cmos distributed sensor system for high-density wireless neural implants for brain-machine interfaces," in *ESSCIRC 2018-IEEE 44th European Solid State Circuits Conference (ESSCIRC)*. IEEE, 2018, pp. 230–233.

[11] Y. Karimi, A. Khalifa, W. Montlouis, M. Stanaćević, and R. Etienne-Cummings, "Coil array design for maximizing wireless power transfer to sub-mm sized implantable devices," pp. 1–4, 2017.

[12] M. Zaeimbashi, M. Nasrollahpour, A. Khalifa, A. Romano, X. Liang, H. Chen, N. Sun, A. Matyushov, H. Lin, C. Dong *et al.*, "Ultra-compact dual-band smart nems magnetoelectric antennas for simultaneous wireless energy harvesting and magnetic field sensing," *bioRxiv*, 2020.

[13] H. Dinis and P. Mendes, "A comprehensive review of powering methods used in state-of-the-art miniaturized implantable electronic devices," *Biosensors and Bioelectronics*, p. 112781, 2020.

[14] F. Rangriz, A. Khaleghi, and I. Balasingham, "Wireless link for micro-scale biomedical implants using magnetoelectric antennas," in *2020 14th European Conference on Antennas and Propagation (EuCAP)*. IEEE, 2020, pp. 1–4.

[15] A. Khalifa, Y. Karimi, Y. Huang, M. Stanaćević, and R. Etienne-Cummings, "The challenges of designing an inductively coupled power link for um-sized on-chip coils," in *2018 IEEE Biomedical Circuits and Systems Conference (BioCAS)*. IEEE, 2018, pp. 1–4.

[16] M. Zargham and P. G. Gulak, "Maximum achievable efficiency in near-field coupled power-transfer systems," *IEEE Transactions on Biomedical Circuits and Systems*, vol. 6, no. 3, pp. 228–245, 2012.

[17] P. Feng, P. Yeon, Y. Cheng, M. Ghovanloo, and T. G. Constandinou, "Chip-scale coils for millimeter-sized bio-implants," *IEEE transactions on biomedical circuits and systems*, vol. 12, no. 5, pp. 1088–1099, 2018.

[18] T. Nan, H. Lin, Y. Gao, A. Matyushov, G. Yu, H. Chen, N. Sun, S. Wei, Z. Wang, M. Li *et al.*, "Acoustically actuated ultra-compact nems magnetoelectric antennas," *Nature communications*, vol. 8, no. 1, p. 296, 2017.